Editors' Suggestion

Data-assimilated low-order vortex modeling of separated flows

Darwin Darakananda,[1] André Fernando de Castro da Silva,[2]
Tim Colonius,[2] and Jeff D. Eldredge[1,*]
[1]*Mechanical and Aerospace Engineering Department, University of California, Los Angeles, Los Angeles, California 90095, USA*
[2]*Mechanical and Civil Engineering Department, California Institute of Technology, Pasadena, California 91125, USA*

(Received 27 August 2018; published 13 December 2018)

Vortex models have been used for decades as computationally efficient tools to investigate unsteady aerodynamics. However, their utility for separated flows—particularly when such flows are subjected to incident disturbances—has been hindered by the tradeoff between the model's physical fidelity and its expectation for fast prediction (e.g., relative to computational fluid dynamics). In this work, it is shown that physical fidelity and speed can be simultaneously achieved by assimilating measurement data into the model to compensate for unrepresented physics. The underlying inviscid vortex model captures the transport of vortex structures with a standard collection of regularized vortex elements that interact mutually and with an infinitely thin flat plate. In order to maintain a low-dimensional representation, with fewer than $O(100)$ degrees of freedom, an aggregation procedure is developed and utilized in which vortex elements are coalesced at each time step. A flow state vector, composed of vortex element properties as well as the critical leading-edge suction parameter, is advanced within an ensemble Kalman filter (EnKF) framework. In this framework, surface pressure is used to correct the states of an ensemble of randomly initiated vortex models. The overall algorithm is applied to several scenarios of an impulsively started flat plate, in which data from a high-fidelity Navier-Stokes simulation at Reynolds number 500 are used as a surrogate for the measurements. The assimilated vortex model efficiently and accurately predicts the evolving flow as well as the normal force in both the undisturbed case (a separated flow) as well as in the presence of one or more incident gusts, despite lack of *a priori* knowledge of the gust's characteristics.

DOI: 10.1103/PhysRevFluids.3.124701

I. INTRODUCTION

The closed-loop control of the separated flow over an airfoil is essential for the development of highly agile aircraft whose flight is robust to disturbances. All control strategies rely fundamentally on an aerodynamics model that can accurately predict the force (and flow) response of an airfoil to arbitrary disturbances and/or actuation and which can be run in real time. Unfortunately, classical linearized quasisteady and impulse response aerodynamic models have difficulty capturing the intrinsically nonlinear response that is observed when a separated flow is subjected to a broad spectrum of disturbances or actuation [1]. Thus, it is natural to consider phenomenological models that can capture this nonlinearity in a direct—but inexpensive—manner. For this purpose, inviscid

*jdeldre@ucla.edu

vortex models, in which advecting vortex elements represent the time-varying flow field through their mutually induced velocities, are a candidate.

Inviscid vortex models have been in common use in recent years to predict the dynamic response of a flow that tends to separate at the leading edge. One class of methods models the flux of vorticity into the wake by a continual release of constant-strength vortex elements from one or both edges of the airfoil [2–4]. As the number of vortex elements increases, their interactions with each other result in the emergence of large-scale structures. These methods have been successful in modeling the detailed physics of the development of dynamic stall and the wake, but at the cost of tracking hundreds to thousands of vortices and their interactions. The continual increase of computational elements makes this class of vortex models impractical as state estimators in closed-loop flow control.

Another class of inviscid vortex models handle vorticity flux through point vortices with time-varying strength [5–8]. In these models, the dominant leading and trailing edge vortices are each modeled with a single point vortex. The roll-up of the shear layers into large-scale structures is captured by increasing the magnitude of the point vortices' circulation. While the low number of computational elements make this class of methods more suitable for real-time applications, the resulting model lacks crucial flow physics. Without an explicit representation for the shear layers that emerge from the edges of the wing, these variable-strength vortex models cannot capture the transformation of a shear-layer instability into a new coherent vortex. To ease the tradeoff between flow physics and computational cost, Darakananda and Eldredge [9,10] developed a hybrid representation in which the evolution of a vortex sheet rooted at each edge of a flat plate accounts for the natural roll-up of emerging vortex structures, and these structures are represented by variable-strength point vortices that siphon their strength from the end of each corresponding sheet. To ensure that this transfer does not spuriously affect the predicted aerodynamic force, an impulse matching principle, developed by Wang and Eldredge [8], was used to adjust the velocity of each variable-strength vortex.

A key open problem in vortex modeling is determining how much vorticity to release from the leading edge. While it is generally accepted that the Kutta condition is an acceptable vortex shedding criterion to use at the trailing edge, its use at the leading edge in numerous vortex models [2,5,8] has not led to good results and this has driven the exploration of empirically determined leading-edge shedding criteria. In the discrete vortex model developed by Katz [11], leading-edge shedding was tuned with a handful of parameters. Some parameters, such as the position of the leading-edge separation point, were chosen based on experimental data, while others were adjusted to bring the predicted force closer to the measured force. In more recent work, Ramesh and Gopalarathnam [3,12] introduced a shedding criterion based on the observation that real airfoils can support a modest level of suction around the leading edge before flow separation is triggered. Correspondingly, the authors suggested the use of the leading-edge suction parameter (LESP), a nondimensional measure of the integrated pressure at the nose of the airfoil, to govern vortex shedding. In their model, when the LESP is below a critical value, which we will denote as LESP_c, no vorticity is released. However, when the instantaneous LESP exceeds LESP_c, vortex elements will be released with the appropriate amount of strength to bring the LESP down to LESP_c. By tuning their discrete vortex model with an empirically determined static value of LESP_c, the authors were able to predict lift responses that were in good agreement with experimental results for several (undisturbed) canonical motions of the wing.

This lack of an obvious theoretical closure in the low-order model at the leading edge has also motivated the development of "data-assisted" vortex models, which are guided in part by measurements from the real system (the "truth"). For example, Hemati *et al.* [13] posed the combination of vortex model and truth measurements as a constrained optimization problem. In this perspective, the leading- and trailing-edge vorticity fluxes were interpreted as inputs to a nonlinear dynamical system. Variational methods were used to compute the time histories of these fluxes that would minimize the squared error between the empirically measured and model-predicted forces over a time horizon, subject to the constraint that the vortex elements move according to their

usual dynamics. They applied this principle to optimize the variable-strength vortex model of Wang and Eldredge [8] using empirical force data from a high-fidelity simulation of the Navier-Stokes equations. While this optimization technique produced good results, it requires the measurements to be available over the entire optimization window. So while it is a useful postprocessing tool, it is also not directly applicable for real-time estimation. In order to overcome this limitation, Darakananda and Eldredge [14] developed a "bootstrapping" procedure that applied the optimization over short time increments, accelerated by an initial guess obtained by regressing over previous time increments. However, in either form, this optimization framework relies on measurements of aerodynamic force from the truth case. These measurements are generally unavailable and indeed comprise part of the state that we seek to predict.

To address the shortcomings of previous approaches, in this paper, we address the problem from the perspective of *data assimilation* and investigate whether it is feasible to use real-time (and possibly noisy) sensor measurements to improve the prediction of a vortex model. To facilitate a more practical estimation strategy, we will only rely on surface pressure measurements, which will be folded into the predictive model through a Kalman filter (KF) framework. The KF framework consists of a predictive step, in which the state of the system is evolved with a dynamical model, followed by a measurement update step, in which the state is corrected based on new observations. Both the state's mean and its covariance matrix—essential for determining the degree to which measurements shall affect the state estimate—are directly propagated in this framework. However, the requirements of tracking the covariance matrix render the algorithm intractably expensive for the moderate- to high-dimensional systems in fluid flows. Thus, in this work, we will utilize an ensemble Kalman filter (EnKF), which was originally conceived to handle the high-dimensional nonlinear dynamics found in meteorology [15]. The EnKF obtains the covariance, as well as the mean state, from an ensemble of randomly initiated instances of the state vector.

The EnKF has recently been investigated for its use in aerodynamics by da Silva and Colonius [16], in which the state prediction was obtained from a finite-volume Navier-Stokes simulation. In the present work, state prediction will be obtained from a discrete vortex element model. To enable the vortex element model to work for wide range of angles of attack, we use the LESP criterion introduced by Ramesh and Gopalarathnam [12], where the leading-edge vorticity flux is determined by a critical LESP. The state vector for the EnKF will be composed of the positions and strengths of all vortex elements, as well as—crucially—the current estimate of the value of LESP_c. Thus, rather than assuming some prior knowledge of LESP_c, we will seek to estimate its value from the measured pressures. To ensure that the length of the state vector remains modest, we will aggregate the vortex elements by a procedure that we will describe in the appendix. The performance of this flow estimation framework will be assessed on undisturbed and disturbed separated flows past a flat plate, using high-fidelity numerical simulations as the truth from which pressure measurements are sampled.

II. METHODOLOGY

In this section, we present our data-assimilated vortex model. The underlying vortex model we use is identical to the method introduced by Ramesh *et al.* [3], aside from the aggregation procedure that we describe in the appendix. The dynamics of the flow are obtained by a standard collection of advecting regularized vortex elements (blobs) about an infinitely thin flat plate. The Kutta condition is enforced at the trailing edge of the plate, while the leading-edge vorticity flux is governed by the LESP criterion. The critical LESP represents a measure of the tolerance for leading-edge suction that does not lead to the flux of new vorticity into the fluid; a critical LESP equal to zero is equivalent to enforcing a Kutta condition at the leading edge. If the instantaneous LESP exceeds the critical value, then a vortex element is released from the edge, with strength proportional to the amount by which LESP_c has been exceeded. Ramesh *et al.* [3] chose a single value for LESP_c from *a priori* comparisons between the vortex model and high-fidelity Navier-Stokes simulations. In contrast, in this work we estimate the value of LESP_c within the data assimilation framework. It is important to

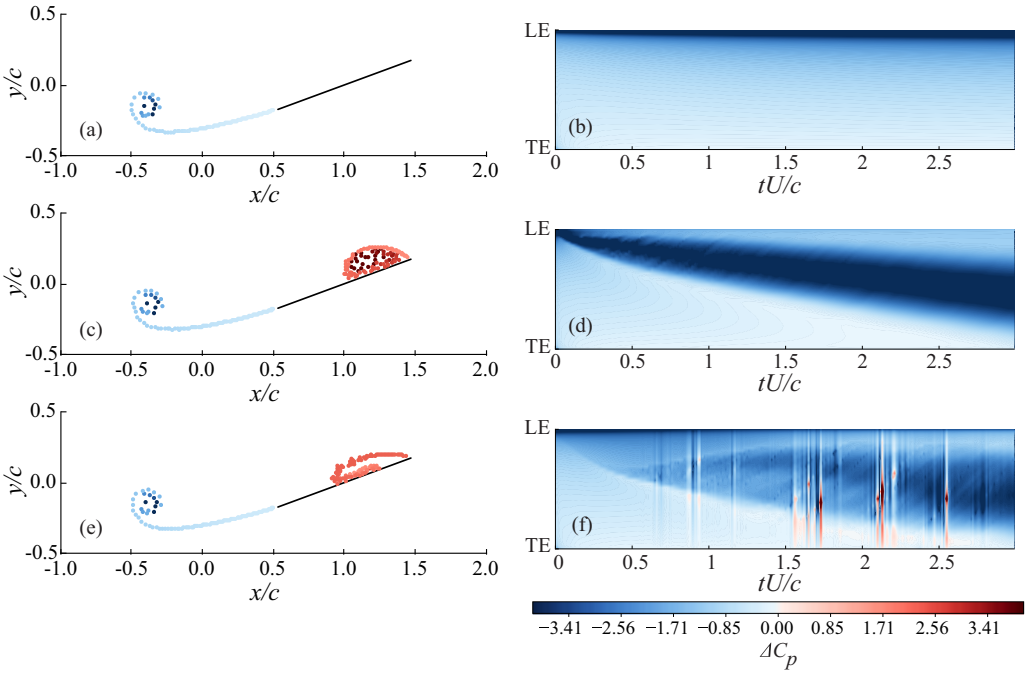

FIG. 1. Comparison of vortex element distributions (left) and surface pressure coefficient distributions (right) predicted by a vortex blob model with different LESP_c values after one convective time. [(a), (b)] $\mathrm{LESP}_c = 3.0$, [(c), (d)] $\mathrm{LESP}_c = 0.3$, and [(e), (f)] $\mathrm{LESP}_c = 0.8$. In each surface pressure coefficient distribution panel, the top of the panel represents the leading edge of the plate, the bottom represents the trailing edge, and the horizontal axis represents the time (in convective units).

note that, since LESP_c determines the flux of vorticity from the leading edge, and subsequently, the flow field dynamics and their effect on surface pressure, it is expected that measurements of surface pressure should inform appropriate values of LESP_c.

A. The critical leading-edge suction parameter

In order to provide some insight for the role of critical LESP, in Fig. 1 we depict a snapshot of the evolving vortex element distribution and the history of the surface pressure distribution for three different constant values of LESP_c for a plate set into translation at 20° angle of attack; this configuration will be one of the target problems of our studies in Sec. III. The surface pressure shown here, as well as in every other pressure plot in this paper, is the difference in pressure coefficient, $\Delta C_p = 2(p^+ - p^-)/\rho U^2$, between the upper $(+)$ and lower $(-)$ surface of the plate; negative values of this coefficient represent suction.

It is important to stress that the choices for LESP_c depicted here are made to explore the flow dynamics under different static values; none is necessarily correct. In the top row, $\mathrm{LESP}_c = 3.0$. Recalling that there must be a sufficiently large leading-edge suction to exceed this critical value, an alternative interpretation of the value is as a critical angle of attack below which the flow is deemed to be attached at the leading edge. Though the instantaneous LESP depends on the full instantaneous flow state, in the absence of ambient vorticity it is solely determined by the angle of incidence of the flow. The critical angle of attack corresponding to $\mathrm{LESP}_c = 3.0$ is larger than 20 deg, so no vorticity is ever released. In the surface pressure plot, in which the vertical axis corresponds to the streamwise spatial direction (with flow from top to bottom) and the horizontal axis represents time, the lack of a leading-edge vortex (LEV) is reflected by a persistent low (suction) pressure in the

vicinity of the leading edge. In contrast, in the middle row, where $\mathrm{LESP}_c = 0.3$, we see that the model predicts the formation of a coherent LEV. This strong LEV exerts a low pressure on the plate immediately below it as the vortex convects toward the trailing edge and relieves the low pressure near the leading edge.

These first two cases illustrate the ends of the spectrum of possibilities for critical LESP. In the lower row of Fig. 1, we take $\mathrm{LESP}_c = 0.8$, and consequently observe the emergence of a weaker LEV. Because the vortex elements released at the leading edge are relatively weak, they are advected closer to the plate surface. Without a viscous boundary layer to absorb this vorticity, the vortex elements create unphysical, impulsive pressure disturbances along the surface.

From these plots of evolving surface pressure distribution, we can clearly see differences in the growth (or absence) of the LEV for different values of LESP_c. This suggests that it may be possible to estimate LESP_c if we are given the surface pressure information. It is important to note that, in this estimation process, we need not assume that the LESP_c remains constant. In this time-varying form, the underlying physical role of LESP_c as a trigger for and moderator of vorticity flux from the leading edge is generalized, so that it can respond to disturbances of various sorts—incident gusts, wing maneuvers, or leading-edge actuators. The estimated value can then be used to close the vortex model and thereby fill in the rest of the evolving flow state. In other words, we seek to assimilate surface pressure measurements in order to estimate one or more missing parameters in our model. We might also be able to use these measurements to improve the estimates of other state variables that are predicted by the vortex model, such as the vortex element positions and strengths.

As with most other inviscid vortex models, the dimension of the system increases with every time step due to the release of new vortex elements from the edge(s) of the body. The steady and unbounded increase of the state dimension prevents such models from being used in any real-time applications. This is essentially the same problem that the hybrid vortex sheet and point vortex model [10] was constructed to solve. Unfortunately, while the hybrid model performs well for high angle of attack and pitchup problems, its use of contiguous vortex sheets makes it less suited for flows at low angles of attack. In the context of the discrete vortex blob method used in the present work, we will instead aggregate blobs at each step in order to maintain a modest population of vortex elements. The aggregated vortex elements are farther from the plate, avoiding the nonphysical interactions observed above. We defer the details of the aggregation method to the appendix, and focus on the data assimilation component of the method.

B. Ensemble Kalman filter approach

We use a Kalman filter (KF) framework in order to algorithmically assimilate surface pressure measurements into the vortex model, as we will describe below. The classical Kalman filter is derived for linear systems. For weakly nonlinear systems, it is popular to use the extended Kalman filter (EKF) [17], in which the nonlinear operators are linearized about the current state. However, the linearization can lead to unstable growth of the error covariance. While this can be solved by using higher order derivatives, the number of terms in the higher order Taylor expansion grows substantially, which can make the computation prohibitively expensive for real-time applications. For the present work, we will use the ensemble Kalman filter (EnKF). The EnKF was introduced by Evensen [15] to explicitly address two key shortcomings in the EKF: the need for explicit Jacobians of the dynamical model and measurement function and the large computational cost for high-dimensional systems.

1. Summary of the EnKF

In this section, we provide an overview of the ensemble Kalman filter; further details, including several practical aspects for computing the Kalman gain from the ensemble statistics, can be found in da Silva and Colonius [16]. The EnKF is essentially a Monte Carlo version of the classical Kalman filter. Instead of describing the distribution of the system state using a mean and a covariance, as in the classical and extended forms of the KF, we approximate the distribution using

an ensemble of size N of randomly initiated members, where the state of the ith member at filter step k is denoted by $\tilde{\boldsymbol{x}}_{i,k}$. Suppose we know the ensemble states at step $k-1$. We can then propagate each member of the ensemble forward in time with a dynamical update (e.g., in the present work, a time-discretized vortex model)

$$\tilde{\boldsymbol{x}}_{i,k}^{-} = \boldsymbol{f}(\tilde{\boldsymbol{x}}_{i,k-1}) \quad \text{for } i = 1, 2, \ldots, N, \tag{1}$$

where the superscript "$-$" indicates that no measurements have been incorporated yet. Note that there is no process noise term in this update equation; this noise will be addressed in the next section when we discuss covariance inflation. We now approximate the premeasurement mean and covariance of the state with their sample values

$$\hat{\boldsymbol{x}}_{k}^{-} := \frac{1}{N}\sum_{i=1}^{N} \tilde{\boldsymbol{x}}_{i,k}^{-} \tag{2}$$

and

$$\boldsymbol{P}_{k}^{-} := \frac{1}{N-1}\sum_{i=1}^{N} (\tilde{\boldsymbol{x}}_{i,k}^{-} - \hat{\boldsymbol{x}}_{k}^{-})(\tilde{\boldsymbol{x}}_{i,k}^{-} - \hat{\boldsymbol{x}}_{k}^{-})^{T}. \tag{3}$$

In the standard forms of the Kalman filter, the innovation—the discrepancy between the predicted measurements and those obtained from the true system, denoted by the vector $\boldsymbol{z}_k$—is defined as

$$\boldsymbol{y}_k := \boldsymbol{z}_k - \boldsymbol{H}_k \hat{\boldsymbol{x}}_{k}^{-}. \tag{4}$$

To adapt this definition to each ensemble member, we replace $\hat{\boldsymbol{x}}_{k}^{-}$ with the ensemble's own dynamical estimate, $\tilde{\boldsymbol{x}}_{i,k}^{-}$. However, we cannot use the same measurement $\boldsymbol{z}_k$ for all ensemble members, as Burgers *et al.* [18] found that doing so in an ensemble ignores the fact that $\boldsymbol{z}_k$ is a random variable and thus introduces spurious correlations in the ensemble covariance. Instead, we must artificially introduce noise into the innovation of each member of the ensemble

$$\boldsymbol{y}_{i,k} := \boldsymbol{z}_k + \boldsymbol{\epsilon}_i - \boldsymbol{H}_k \tilde{\boldsymbol{x}}_{i,k}^{-} \quad \text{for } i = 1, 2, \ldots, N, \tag{5}$$

where the $\boldsymbol{\epsilon}_i$ are vectors of random numbers drawn from a normal distribution with zero mean and covariance $\boldsymbol{V}_k$. The Kalman update step is then applied to each member of the ensemble

$$\tilde{\boldsymbol{x}}_{i,k} := \tilde{\boldsymbol{x}}_{i,k}^{-} + \boldsymbol{K}_k(\boldsymbol{z}_k + \boldsymbol{\epsilon}_i - \boldsymbol{H}_k \tilde{\boldsymbol{x}}_{i,k}^{-}) \quad \text{for } i = 1, 2, \ldots, N, \tag{6}$$

where the Kalman gain has its usual form,

$$\boldsymbol{K}_k = \boldsymbol{P}_k^{-} \boldsymbol{H}_k^{T} \left(\boldsymbol{V}_k + \boldsymbol{H}_k \boldsymbol{P}_k^{-} \boldsymbol{H}_k^{T}\right)^{-1}. \tag{7}$$

Thus, while all members of the ensemble share the same Kalman gain, they each have a unique innovation.

2. Covariance inflation

The EnKF, like the original Kalman filter, is constructed to minimize the final covariance, $\boldsymbol{P}_k$, of the estimated state distribution. In the Kalman filter, information about the process noise and measurement noise are accounted for via their respective covariances, $\boldsymbol{W}_k$ and $\boldsymbol{V}_k$, in the evolved state covariance matrix. In the EnKF, this process noise is independently sampled from $\boldsymbol{W}_k$ and explicitly added to the ensemble members in the EnKF, comprising a Monte Carlo formulation of the Kalman filter. In the absence of such added noise, the system variance decreases to a lower bound determined only by the measurement covariance, $\boldsymbol{V}_k$, so that the estimator cannot distinguish measurement noise from state uncertainty. As a result, the Kalman gain of the ensemble becomes minimally small, so that new measurements are effectively ignored by the filter. All members of the ensemble become essentially identical to one another. This so-called covariance collapse can be desirable in circumstances in which the dynamical model is completely deterministic and the filter

has gathered sufficient data to locate the system's position in state space. However, in the context of the EnKF, it generally leads to a significant underestimate of the state covariance and suboptimal measurement corrections.

A class of methods for handling this covariance collapse is called covariance inflation. In general, covariance inflation modifies the ensemble states before computing the sample mean and covariance. Each ensemble state is updated by

$$\tilde{\boldsymbol{x}}_{i,k}^{-} \leftarrow \hat{\boldsymbol{x}}_{k}^{-} + \beta(\tilde{\boldsymbol{x}}_{i,k}^{-} - \hat{\boldsymbol{x}}_{k}^{-}) + \boldsymbol{\alpha}_{i,k}, \tag{8}$$

where β is the multiplicative inflation factor shared among all ensemble members and $\boldsymbol{\alpha}_{i,k}$ is the additive inflation factor drawn from a random distribution at each filter step and independently for each ensemble member [19–21]. After this update, we recompute the ensemble mean and compute the ensemble covariance. Whitaker and Hammill [21] found that multiplicative inflation tends to be better at countering the effects of sampling errors, while additive inflation tends to be better at accounting for modeling errors. Multiplicative inflation tends to be easier to tune as it only involves adjusting a single value. Adjusting additive inflation, in contrast, requires more understanding about the actual dynamics of the underlying system.

3. Applying the EnKF to a vortex model

The state vector of our EnKF-assisted vortex model consists of the positions and strengths of the n vortex blobs, as well as the current estimate of the LESP_c:

$$\boldsymbol{x}_{k-1} := \begin{bmatrix} x_{k-1}^1 & y_{k-1}^1 & \Gamma_{k-1}^1 & \dots & x_{k-1}^n & y_{k-1}^n & \Gamma_{k-1}^n & \mathrm{LESP}_{k-1}^c \end{bmatrix}^T. \tag{9}$$

The nonlinear state transition function $\boldsymbol{f}_k$ propagates the state from step $k-1$ to step k by the following method:

(1) computing the bound vortex sheet strength on the plate from the no-penetration condition, using the current vortex blob positions and strengths;

(2) computing the velocities of the vortex blobs;

(3) advecting the plate and the vortex blobs;

(4) applying the vortex aggregation algorithm, reducing the strength of any aggregated blobs to zero instead of completely removing the blob; and

(5) releasing a new vortex blob from each edge of the plate with strengths based on the Kutta condition at the trailing edge and the current estimate of the LESP_c (similar to Ramesh *et al.* [3]) at the leading edge.

Note that the dimension of the state vector increases by six (three per new vortex blob) after every state propagation step. Once all members of the ensemble have been propagated, we look for any vortex blobs that have zero strength across *all* members of the ensemble (in terms of its position and/or index in the state vector) and eliminate them from the ensemble states. This element elimination process, in conjunction with the vortex aggregation algorithm, keeps the dimension of the state vector in check. However, by requiring that all ensemble members unanimously agree on an element's irrelevance, we ensure that the state vector has uniform dimensionality across all members. We then apply covariance inflation to the new ensemble states, before computing the premeasurement ensemble mean $\hat{\boldsymbol{x}}_{k}^{-}$ and ensemble covariance $\boldsymbol{P}_{k}^{-}$ with Eqs. (2) and (3).

Our measurements consist of M pressure differences between the upper and lower surfaces of the plate at every filter step k,

$$\boldsymbol{z}_k := \begin{bmatrix} \Delta p_k^1 & \dots & \Delta p_k^M \end{bmatrix}^T. \tag{10}$$

Let us denote the vector of pressure differences predicted by the ith ensemble member at filter step k by

$$\boldsymbol{m}_{i,k} := \boldsymbol{h}_k(\tilde{\boldsymbol{x}}_{i,k}^{-}). \tag{11}$$

Then the innovation for each member of the ensemble is given by

$$\boldsymbol{y}_{i,k} = \boldsymbol{z}_k + \boldsymbol{\epsilon}_i - \boldsymbol{m}_{i,k}. \tag{12}$$

Since pressure is not a linear function of vortex element properties, we need to develop a linear form of the measurement function $\boldsymbol{h}_k$ in order to compute the ensemble Kalman gain. One simple way to achieve this is to define an augmented state vector containing the measurements themselves

$$\boldsymbol{X}_{i,k} := \begin{bmatrix} \tilde{\boldsymbol{x}}^-_{i,k} \\ \boldsymbol{m}_{i,k} \end{bmatrix}, \tag{13}$$

which admits the linear measurement function

$$\boldsymbol{H}_k := [\boldsymbol{0}^{(3n+1)\times(3n+1)} \quad \boldsymbol{I}^{M\times M}], \tag{14}$$

where $\boldsymbol{I}^{M\times M}$ is the M-dimensional identity matrix. Then, denoting the mean of the predicted pressure distribution by

$$\bar{\boldsymbol{m}}_k := \frac{1}{N}\sum_{i=1}^{N} \boldsymbol{m}_{i,k}, \tag{15}$$

the covariance of the predicted pressure distribution by

$$\boldsymbol{M}_k := \frac{1}{N-1}\sum_{i=1}^{N} (\boldsymbol{m}_{i,k} - \bar{\boldsymbol{m}}_k)(\boldsymbol{m}_{i,k} - \bar{\boldsymbol{m}}_k)^T, \tag{16}$$

and the cross covariance between the state and pressure with

$$\boldsymbol{C}_k := \frac{1}{N-1}\sum_{i=1}^{N} (\tilde{\boldsymbol{x}}^-_{i,k} - \hat{\boldsymbol{x}}_k)(\boldsymbol{m}_{i,k} - \bar{\boldsymbol{m}}_k)^T, \tag{17}$$

we find that the ensemble covariance of the augmented state can be written as

$$\boldsymbol{P}^a_k := \frac{1}{N-1}\sum_{i=1}^{N} \left(\begin{bmatrix} (\tilde{\boldsymbol{x}}^-_{i,k} - \hat{\boldsymbol{x}}_k) \\ (\boldsymbol{m}_{i,k} - \bar{\boldsymbol{m}}_k) \end{bmatrix} [(\tilde{\boldsymbol{x}}^-_{i,k} - \hat{\boldsymbol{x}}_k)^T (\boldsymbol{m}_{i,k} - \bar{\boldsymbol{m}}_k)^T] \right) = \begin{bmatrix} \boldsymbol{P}^-_k & \boldsymbol{C}_k \\ \boldsymbol{C}^T_k & \boldsymbol{M}_k \end{bmatrix}. \tag{18}$$

The Kalman gain of the pressure-augmented system is then

$$\boldsymbol{K}^a_k = \boldsymbol{P}^a_k \boldsymbol{H}^T_k \left(\boldsymbol{V}_k + \boldsymbol{H}_k \boldsymbol{P}^a_k \boldsymbol{H}^T_k\right)^{-1} = \begin{bmatrix} \boldsymbol{C}_k(\boldsymbol{V}_k + \boldsymbol{M}_k)^{-1} \\ \boldsymbol{M}_k(\boldsymbol{V}_k + \boldsymbol{M}_k)^{-1} \end{bmatrix}. \tag{19}$$

Since only the first block in the Kalman gain matrix above corresponds to the actual states we are interested in, we can write the measurement update step for our system as

$$\tilde{\boldsymbol{x}}_{i,k} = \tilde{\boldsymbol{x}}^-_{i,k} + \boldsymbol{C}_k(\boldsymbol{V}_k + \boldsymbol{M}_k)^{-1}[\boldsymbol{z}_k + \boldsymbol{\epsilon}_i - \boldsymbol{h}_k(\tilde{\boldsymbol{x}}^-_{i,k})]. \tag{20}$$

This procedure, proposed by Evensen [22], can be interpreted as an implicit linearization about the ensemble mean.

III. RESULTS

We will demonstrate the EnKF-assisted vortex method on three test problems, each involving a flat plate of chord length c translating at velocity U. Time is measured in typical convective units, $t^* = Ut/c$. In the first two cases, we explore the impulsive translation of the plate at fixed angles of incidence 60° and 20°, respectively. The third case is initiated in the same manner as the 20° case, but two incident disturbances are applied near the leading edge after three and four convective

time units, respectively. The vortex model uses the same estimation framework for this case and is given no additional information about these disturbances other than what is measured in the surface pressure. For all cases, the measurements consist of pressure differences across the plate at $M = 50$ points, distributed symmetrically about the plate centroid at positions

$$\frac{c}{2}\cos\left(\frac{m\pi}{M+1}\right) \quad \text{for } m = 1, 2, \ldots, M. \tag{21}$$

The truth measurements in all cases are obtained from high-fidelity numerical simulation with the immersed-boundary projection method [23] of an infinitely thin flat plate at Reynolds number $\mathrm{Re} = 500$.

Throughout, we use an ensemble size of $N = 50$. The results are not sensitive to this choice of size, but it represents a compromise between statistical convergence (with increasing N) and speed. We initialize each ensemble member with a starting value of LESP_c drawn from a normal distribution $\mathcal{N}(0.5,\ 0.2)$ (i.e., mean 0.5, variance 0.2). (It should be noted that the definition of LESP in the present work is larger by a factor of four than the definition used by Ramesh *et al.* [3].) The covariance inflation parameters are tuned on the 20° impulsive translation case, and take the following values for all cases:

(1) multiplicative inflation is $\beta = 1.01$;

(2) additive perturbations to the vortex positions (normalized by c) are drawn from $\mathcal{N}(0,\ 10^{-5})$;

(3) additive perturbations to the vortex strengths (normalized by Uc) are drawn from $\mathcal{N}(0,\ 10^{-3}\Delta t^*)$;

(4) additive perturbations to the LESP_c are drawn from $\mathcal{N}(0,\ 5 \times 10^{-5})$; and

(5) artificial measurement noise drawn from $\mathcal{N}(0,\ 2.5 \times 10^{-4})$ is added to the truth pressure measurements (nondimensionalized by ρU^2).

These inflation parameters are tuned to coerce the EnKF into favoring the modification of the LESP_c over the vortex element positions and strengths. This stems from our underlying assumption that the key process is still governed by inviscid vortex dynamics, and the assimilation of pressure data via the EnKF is a closure model to determine vorticity flux. Interestingly, although these inflation parameters were tuned for one specific test case, we will see that that same parameters work equally well with the other cases that we will present. For cases in which the vortex aggregation procedure is applied, we set the error tolerance to $\epsilon_F/(\rho U^2 c) = 0.25\Delta t^*$; the role of this tolerance is described in the appendix. The vortex model is advanced with a forward Euler scheme with a fixed time step size of $\Delta t^* = 0.01$. The vortex elements are regularized with a blob radius of $0.005c$. It should be noted that the blob radius does not serve as significant a role in this aggregated model as it does in previous (nonaggregated) vortex models, in which elements are in close proximity and interact strongly with one another. The aggregated vortices are, in contrast, more isolated and their interactions require less regularization. The nonzero blob radius mostly serves to regularize the interactions of elements soon after they are released from the edges; we have found that the results are relatively insensitive to the choice.

A. Impulsive translation at 60°

This high angle of incidence presents a relatively simpler estimation problem than the later case at low angle of incidence because it is expected, from previous experience at high angles [2,4,8,10,24], that a vortex model with the Kutta condition enforced at both edges can provide a reasonably good prediction of the flow behavior. In other words, the data assimilation should have a relatively small role in ensuring an accurate estimate. This case allows us to improve our understanding of the relationships among surface pressure, critical LESP, and the aggregating vortex model, particularly when combined within the EnKF. We will compare the proposed EnKF-assisted vortex model with the high-fidelity numerical simulation at Reynolds number 500 (the "truth" data) and two "unfiltered" versions of the vortex element model with the Kutta condition applied at both edges: a straightforward model and a model with the aggregation scheme applied.

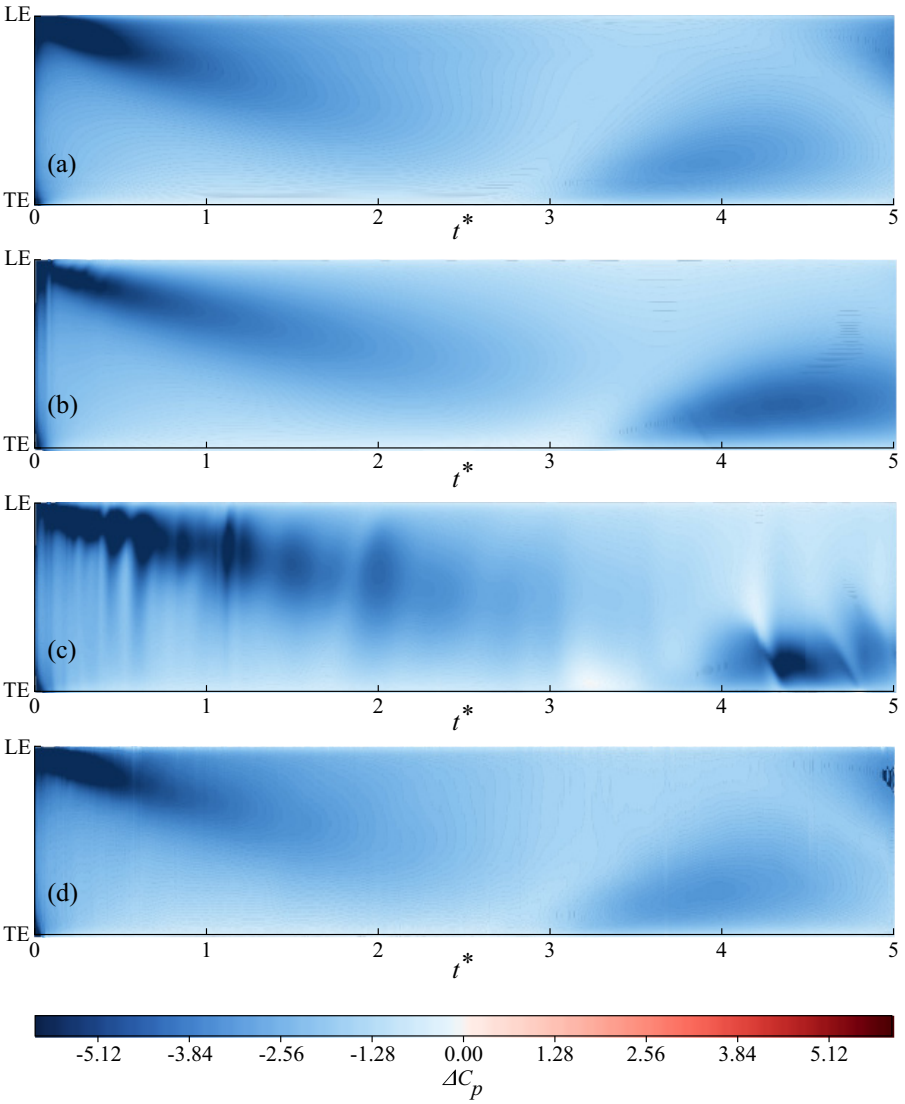

FIG. 2. Comparison of the surface pressure distribution over time along an impulsively translating plate at 60° between (a) high-fidelity simulation, (b) a basic discrete vortex element model, (c) a vortex element model with aggregation, and (d) the proposed EnKF-assisted model. Convective time is defined as $t^* = tU/c$.

The top panel in Fig. 2 shows the pressure distribution from the high-fidelity truth simulation. From visual inspection, we can easily observe the growth and evolution of the LEV, indicated by the expansion of a negative-pressure region moving toward the trailing edge. After the LEV stretches across the whole chord at around two convective times, it starts to entrain opposite-signed vorticity and trigger the development of a trailing-edge vortex, which shows up as a negative-pressure region near that edge between three and five convective times. These events are confirmed in the top left panel of Fig. 3, which depicts the vorticity field from this simulation at $tU/c = 3$. At around $tU/c = 4.5$, a new negative-pressure region at the leading edge indicates the emergence of a new LEV as the trailing-edge vortex starts to entrain positively signed vorticity. This event is evident in the upper right panel in Fig. 3, depicting vorticity after five convective time units.

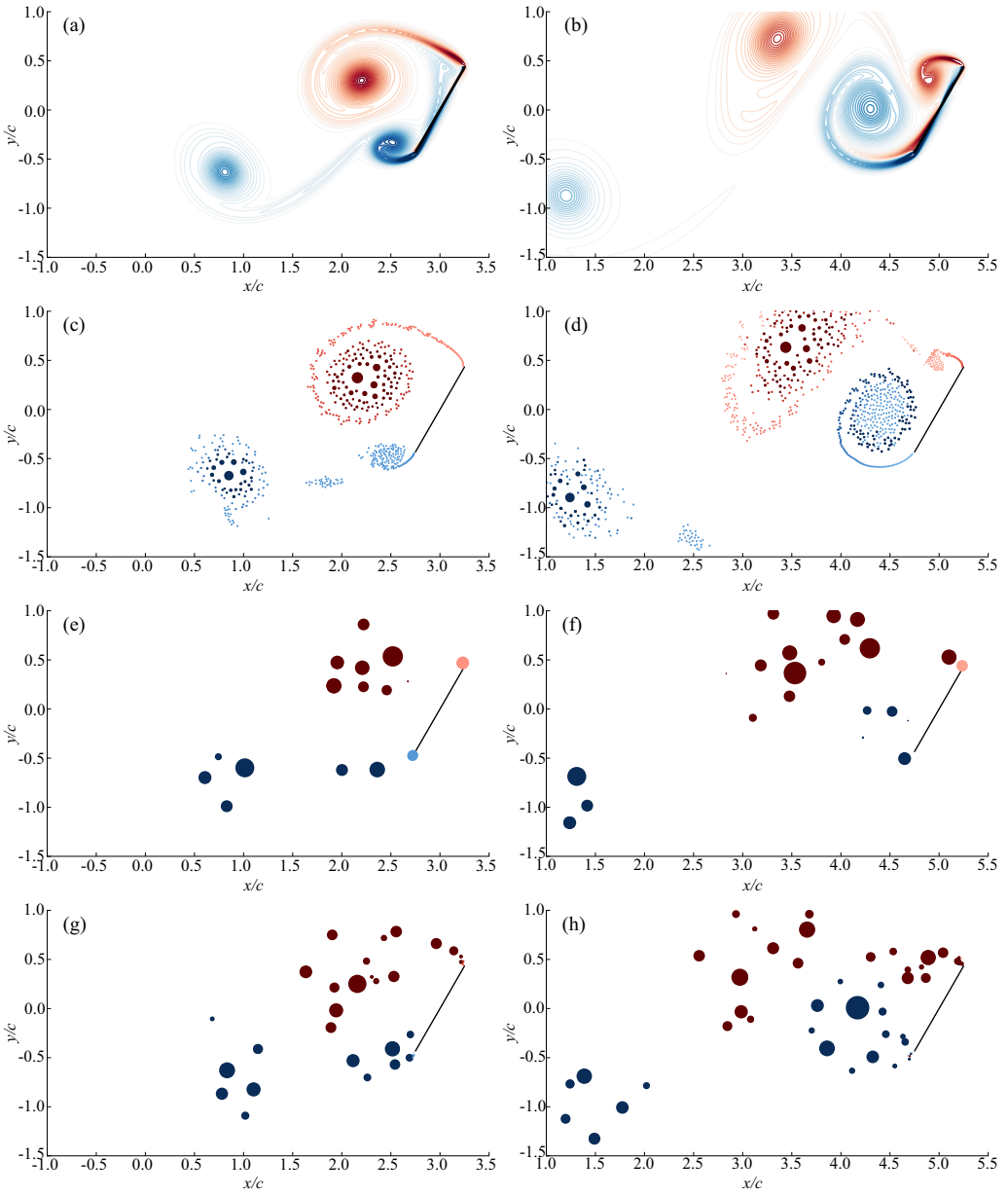

FIG. 3. Comparison of vorticity distribution for the 60° impulsive translation case at $t^* = 3$ (left column) and $t^* = 5$ (right column), predicted by [(a), (b)] high-fidelity simulation, [(c), (d)] a basic discrete vortex element model, [(e), (f)] a vortex element model with aggregation, and [(g), (h)] the proposed EnKF-assisted model.

The overall features of this process are also observable in the basic discrete vortex element simulation, shown in the second rows of Figs. 2 and 3. Indeed, these vortex element results look very similar to those of the truth, except that the trailing-edge suction region is stronger and larger, and there is little evidence in the pressure of the new leading-edge vortex at five convective times. The difference between this prediction and the truth results is more apparent in the normal force coefficient, shown in Fig. 4. The vortex element model predicts a larger force on the plate and

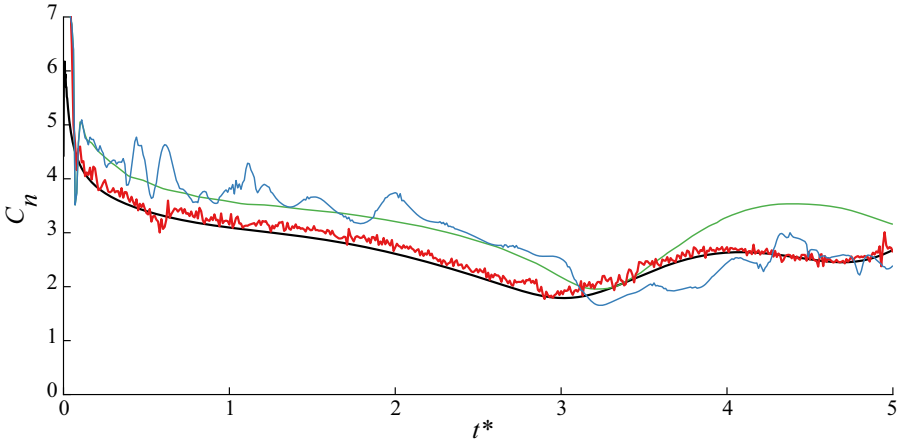

FIG. 4. Comparison of the history of the normal force coefficient (normalized by $\rho U^2 c/2$) on the plate at 60° predicted by the high-fidelity truth simulation (—), a basic discrete vortex element model (—), a vortex element model with aggregation (—), and an EnKF-assisted vortex element model (—).

exhibits a slight lag in the LEV shedding, indicated roughly by the instant at which the force reaches its minimum. It is these differences that we seek to reduce with the assimilation of pressure data.

The use of the vortex element model to predict flow behavior comes at the expense of introducing two new vortex elements per time step; thus, after five convective time units, there are 1000 vortex elements in the system. For an n-body algorithm such as a vortex element method, this rate of growth in the population of computational elements becomes impractically expensive without the use of a fast multipole method. To improve the efficiency, we apply the aggregation scheme described in the appendix to the vortex element method. In the third rows of Figs. 2 and 3, we show, respectively, the surface pressure and snapshots of the vortex element distribution predicted by this aggregated vortex model. The pressure exhibits more oscillations than in the basic (unaggregated) vortex element case, but the same general behavior; the aggregated vortex elements are stronger and appear to coincide with the dominant vortex structures. As is clear from Fig. 3, the high error tolerance (set to the value reported above) has allowed the model to aggressively merge the vortex elements and has thus reduced the element population by almost two orders of magnitude, as seen in Fig. 5. However, as Fig. 4 shows, the aggressive aggregation has also introduced spurious disturbances to the force response.

Finally, we apply the proposed EnKF-assisted aggregated vortex model, using an ensemble of 50 instances of the model. Each member is initialized with no vortex elements—as with any vortex model of an impulsive start in quiescent fluid—and critical LESP values drawn from $\mathcal{N}(0.3,\ 0.2)$.

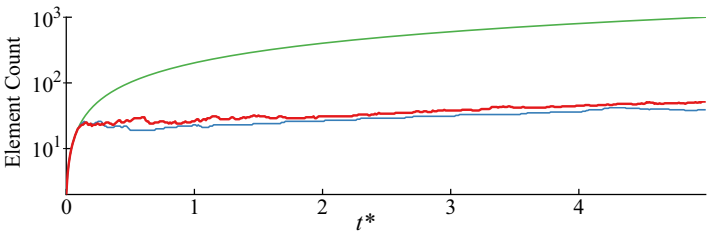

FIG. 5. Number of vortex elements used in vortex models of the impulsively translating plate at 60°. Basic vortex element model (—); aggregated vortex element model (—); EnKF-assisted vortex element model (—).

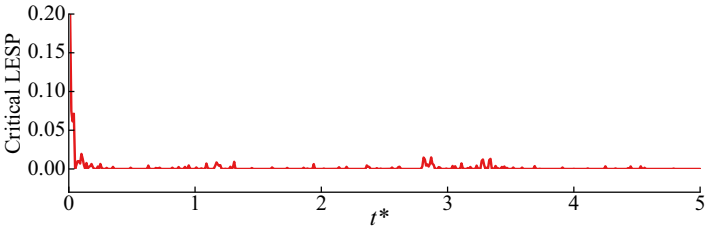

FIG. 6. Time history of the ensemble mean value of LESP_c for the impulsively translating plate at 60° case.

These choices for mean and variance do not require much care, and are only made to ensure a high probability that all ensemble members release vortex elements from the leading edge. The resulting surface pressure distribution history is depicted in the last row of Fig. 2. It is clear that the predicted pressure distribution agrees visually well with the high-fidelity truth simulation. The resulting force of the ensemble mean, plotted in Fig. 4, agrees significantly better than either of the unfiltered vortex models, albeit with some small-amplitude noise due to the variance across the ensemble.

The vortex element distribution of the ensemble mean, shown at two instants in the last row of Fig. 3, is slightly less aggregated than in the previous (unfiltered) case; though the error tolerance is the same, the requirement for unanimous agreement across the entire ensemble restricts the aggregation somewhat. Furthermore, it is important to note that each of the ensemble members has a slightly different version of this same distribution. Indeed, the additive covariance inflation of vortex positions is equivalent to a random walk, used in some previous vortex methods for approximating viscous diffusion [25]. The main differences in the present approach are that the random walk is applied across an ensemble of models and that the vortex strengths are also randomly perturbed. It should be noted, however, that we have not attempted in this work to tune the additive inflation to capture diffusion at this Reynolds number; this relationship will be explored more thoroughly in future work.

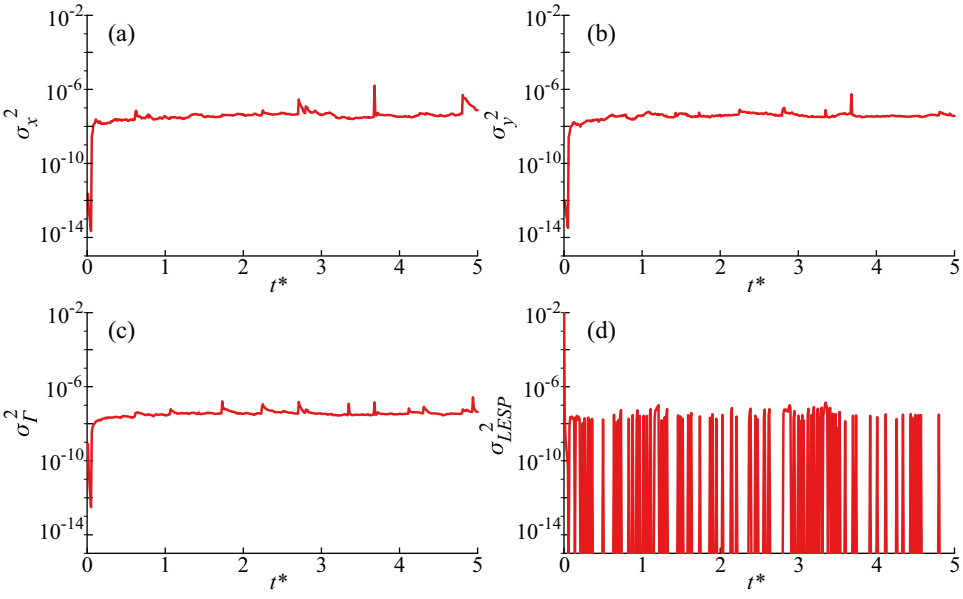

FIG. 7. Ensemble variances for the 60° impulsive translation case. Variances for (a) element x position, (b) element y position, (c) element strength, and (d) critical LESP.

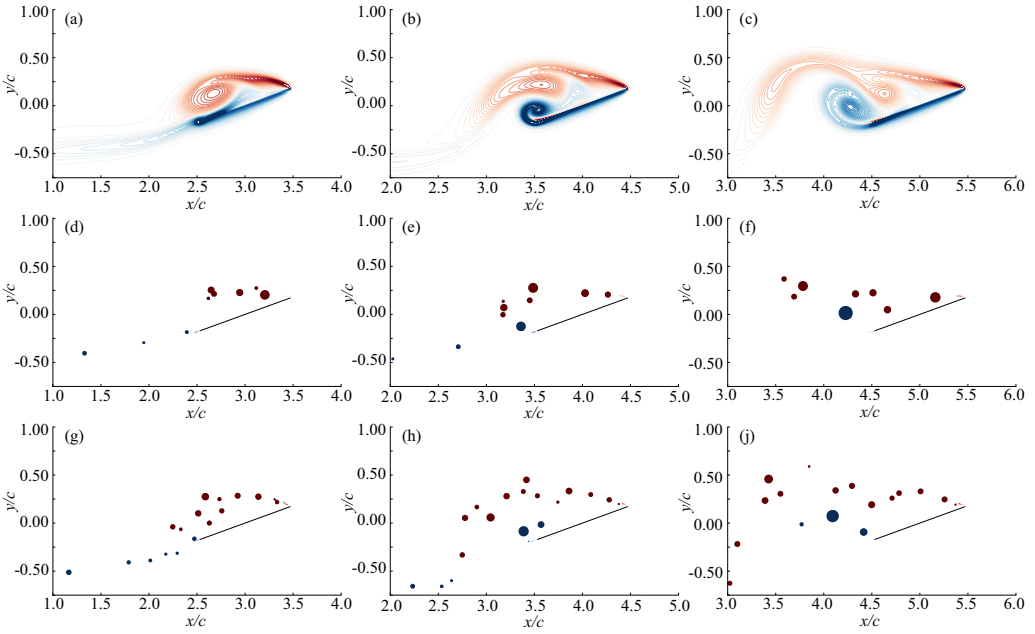

FIG. 8. Vorticity distribution for the 20° impulsive translation case at $t^* = 3$ (left column), $t^* = 4$ (center column), and $t^* = 5$ (right column), from [(a)–(c)] high-fidelity truth simulation at Reynolds number 500, [(d)–(f)] the EnKF-assisted model without inflation, and [(g)–(j)] the EnKF-assisted model with inflation.

The slightly higher population of the ensemble is more directly observable in the plot of element population in Fig. 5. The element distribution predicted by the EnKF-assisted model is more representative of the true vorticity distribution than the unfiltered aggregated vortex model. By assimilating surface pressure data, we obtain better agreement in pressure and force than the basic vortex element model while still using two orders fewer vortex particles.

It is interesting to inspect the ensemble statistics to learn more about how the EnKF has helped achieve this improved estimate. Figure 6 shows the mean critical LESP predicted by the EnKF-assisted model. The critical LESP is constrained to remain non-negative. The initial statistics of the ensemble are apparent in the early values of this parameter. However, it is clear that the EnKF quickly brings LESP_c down to almost zero, which essentially enforces the Kutta condition at the leading edge. This is consistent with the successful use of a leading-edge Kutta condition in previous vortex modeling work at high angles of attack. (Had we applied the model to measurements obtained from a rounded-nose airfoil instead of a flat plate, it is expected, based on the work of Ramesh *et al.* [3], that the estimated value of critical LESP would be nonzero.)

Figure 7 depicts the ensemble variances of the vortex positions, strengths, and critical LESP at the end of each measurement update step. We can see that the variances of the vortex states stay relatively constant over time. As we will see in the next case, the persistence of these values is due to the additive covariance inflation. However, it should be noted that these values are lower than the variances of the normal distribution from which additive inflation values are drawn from, because the Kalman gain in the measurement update step is constructed to minimize these posterior covariances. Furthermore, it is notable that the variance of the estimated critical LESP of the ensemble drops to zero at multiple times. This seems to indicate that, in order to achieve better agreement with the measured pressure data, the EnKF calls for the release of stronger vorticity from the leading edge. Since the maximum flux of vorticity that can be produced by an LESP-based vortex shedding criterion is that dictated by the Kutta condition (where $\mathrm{LESP}_c = 0$), the EnKF drives all ensemble members to a critical LESP value of zero in order to release as much vorticity as

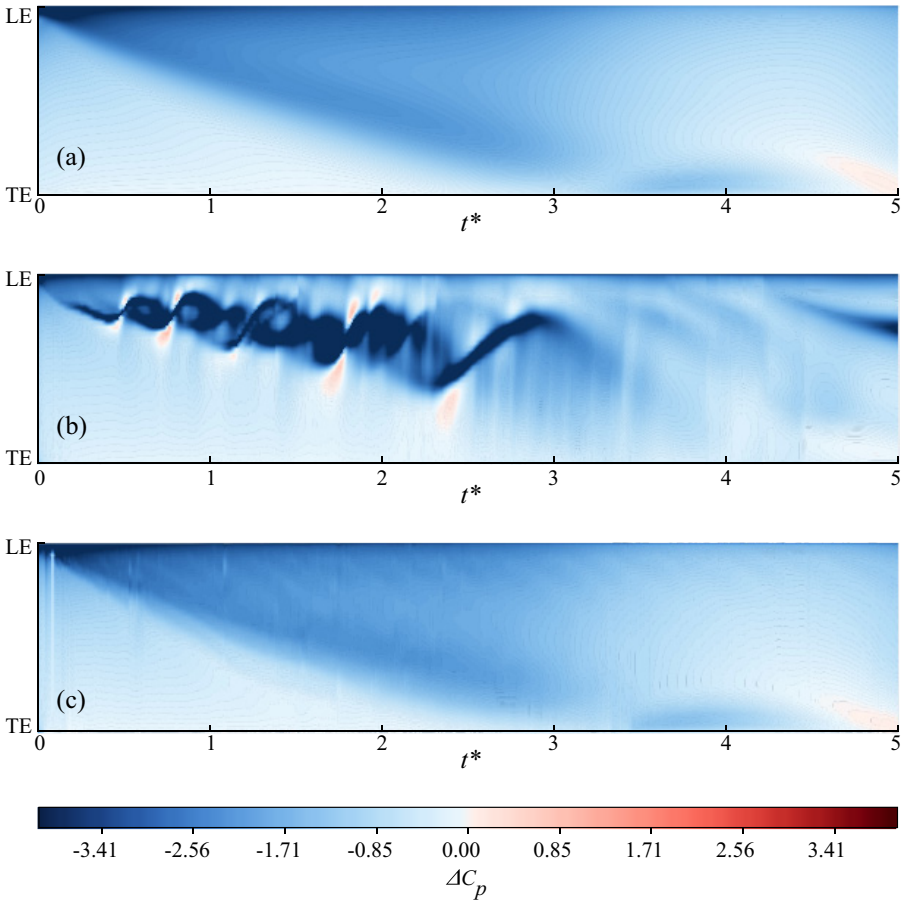

FIG. 9. Histories of the surface pressure distribution along an impulsively translating plate at 20°, from (a) high-fidelity truth simulation at Reynolds number 500, (b) EnKF-assisted model without covariance inflation, and (c) EnKF-assisted model with covariance inflation.

possible. Note that this does not mean that all ensemble members will release a new vortex particle with the same strength, since the strength also depends on the ambient vorticity, which varies among ensemble members.

B. Impulsive translation at 20°

In the previous case, we compared the EnKF-assisted vortex model with unfiltered models. In this case, in which the plate translates impulsively at 20°, we will explore the effects of covariance inflation. Figure 8 depicts snapshots of the vorticity distribution for the high-fidelity truth simulation compared with ensemble averages of vortex elements in two versions of the EnKF-assisted aggregated vortex model, without and with additive covariance inflation, respectively. There are no obvious differences between the two vortex models, except that the version without covariance inflation appears to have fewer elements. Both models' element distributions are qualitatively similar to the vorticity distribution in the high-fidelity truth simulation. However, the differences between the two approaches are much more apparent in the plot of surface pressure history in Fig. 9. With no covariance inflation, the surface pressures are stronger and more compact, with

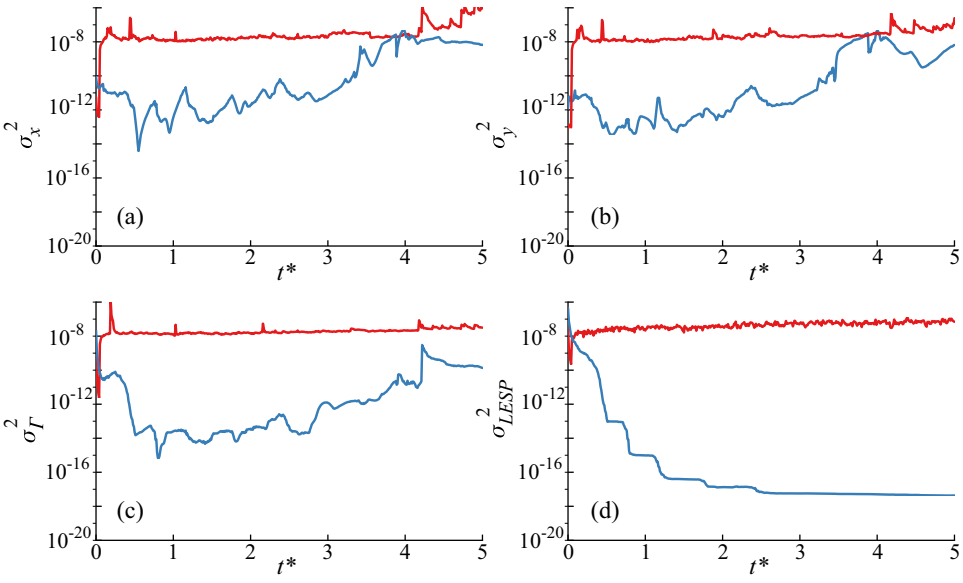

FIG. 10. Ensemble variances for the 20° impulsively translating plate, with no covariance inflation (—) and with covariance inflation (—). Variances for (a) element x position, (b) element y position, (c) element strength, and (d) critical LESP.

features that appear to propagate both upstream and downstream. In contrast, the pressure obtained from the model with inflation is more diffuse and agrees well with the truth data.

The features exhibited in the surface pressure of the noninflated model are typical of a small number of strong vortex elements undergoing dynamics in the vicinity of the plate. The absence of these features in the inflated model is due to the persistent variance among ensemble members: each member's vortex elements are experiencing slightly different dynamics, and the overall effect is a more diffuse pressure field exerted on the plate. This variance nearly vanishes in the noninflated model, as can be observed in Fig. 10. The variances of vortex parameters—positions and strengths—are generally several orders smaller than in the inflated model, though their positional variances exhibit an increase at the end of the interval. Most notably, the variance of LESP_c has completely collapsed, so that all ensemble members are generating nearly the same vorticity flux at the leading edge. As a result of this collapse, the pressure measurements are having little effect on the ensemble. The covariance inflation prevents this collapse, maintaining a truly random ensemble of vortex models of the flow that are actively corrected by the pressure measurements.

The resulting histories of force on the plate, from the truth simulation and from the noninflated and inflated EnKF-assisted vortex models, are depicted in Fig. 11. The force from the inflated model agrees better with the truth data than the noninflated model. Furthermore, the level of noise, due to the influence of dynamical interactions between elements and the errors from continuous aggregation of vortex elements, is somewhat weaker in the inflated model than the noninflated model due to the effect of averaging over the random ensemble. The element populations are only mildly different in the two approaches, as evident in Fig. 12, and both are on the order of tens of elements, much lower than the 1000 elements expected of a basic vortex element model after the same number of time steps. The element population of the inflated model increases at a faster rate than the noninflated model due to greater restriction on the aggregation: Unanimous agreement between ensemble members to aggregate an element pair is harder to achieve when the members maintain differences from one another.

Finally, Fig. 13 depicts the mean estimate of LESP_c obtained from the EnKF-assisted vortex model. Not surprisingly, the noninflated model, with its collapse covariance, converges quickly

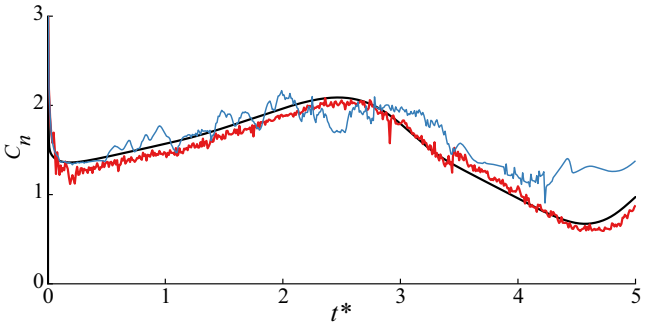

FIG. 11. Comparison of the histories of the normal force coefficient for an impulsively translating plate at 20° from high-fidelity truth simulation (—) and an EnKF-assisted vortex model without covariance inflation (—) and with covariance inflation (—).

to a value and remains nearly fixed. Measurements no longer have an effect, and, in the absence of an underlying dynamical model for critical LESP, there is no other guidance for changing its value. In contrast, the inflated model remains receptive to surface pressure measurements, and these measurements continue to provide information for the instantaneous estimate of LESP_c. After the early transient, this value remains reasonably constant in a range between 0.4 and 0.6; this supports the hypothesis of Ramesh *et al.* [3] that LESP_c is constant for a given wing geometry and Reynolds number. However, a gradual decay in the estimated value is apparent after three convective time units. This decay, which triggers stronger vorticity flux from the leading edge, coincides with the shedding of the original LEV and the development of a new vortex at the leading edge. In other words, for the model to provide accurate estimation over long times, LESP_c must adapt to changing flow conditions.

C. Response to incident disturbances

The previous case confirmed the need for covariance inflation to maintain variance among the vortex models in the ensemble. It also demonstrated that LESP_c may change with the flow conditions, even if the plate's nominal configuration has not changed. In this case, we will evaluate the estimation framework when the plate is subjected to external disturbances, in the form of two "gusts" incident upon the plate. Each gust is introduced to the high-fidelity numerical simulation as a short-duration vertical body force of strength $0.01\rho U^2 c$, applied to the fluid in a small region of the fluid just ahead of the plate, centered at $(0.95c, 0.2\sqrt{\pi}c)$ in plate-centered coordinates. The gusts are introduced, respectively, three and four convective time units after the plate's motion is initiated, and the plate interacts with each as it translates through the disturbance region. It is important to stress that these gusts are only present in the truth simulation; the vortex models in the ensemble

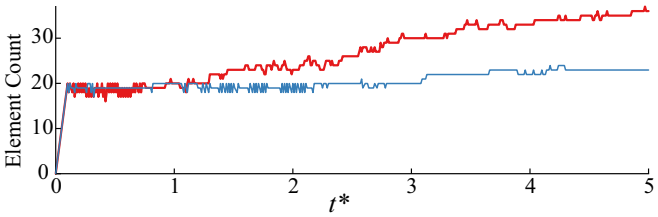

FIG. 12. Number of vortex elements used in the EnKF-assisted model over time for the impulsively translating plate at 20°, without covariance inflation (—) and with covariance inflation (—).

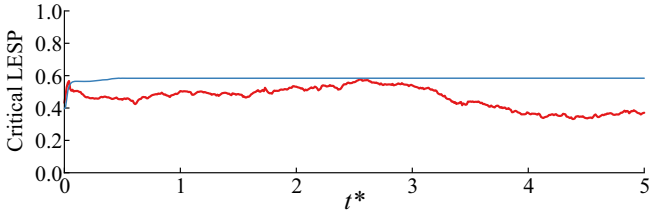

FIG. 13. Time history of the ensemble mean value of LESP_c for the 20° impulsively translating plate, without covariance inflation (—) and with covariance inflation (—).

will have no explicit representation of the gusts. Rather, the models will only "feel" the gust via the measured surface pressures, and then attempt to capture the transient response of the flow to the gust through the resulting corrections to the state vector, which, as before, consists of vortex parameters and LESP_c.

The surface pressure distribution histories for both the truth simulation and the EnKF-assisted vortex model are depicted in Fig. 14. As expected, the initial development of the LEV is identical to the disturbance-free case. At three and four convective time units, we see the gust encounters as bands of negative pressure across the chord. Although the encounters themselves are short-lived, we see that they each trigger the growth of a new LEV. The associated vorticity distributions of the truth simulation are depicted at three instants in the top row of Fig. 15. The first new LEV created around three convective times is advected along the plate and eventually entrained into the initial LEV. At four convective times, the initial LEV has shed from the plate, so that the new LEV created by the second gust remains distinct. The EnKF-assisted vortex model matches the surface pressures well. Furthermore, the vortex elements, depicted at three instants in Fig. 15, accurately track the corresponding flow structures in the truth data.

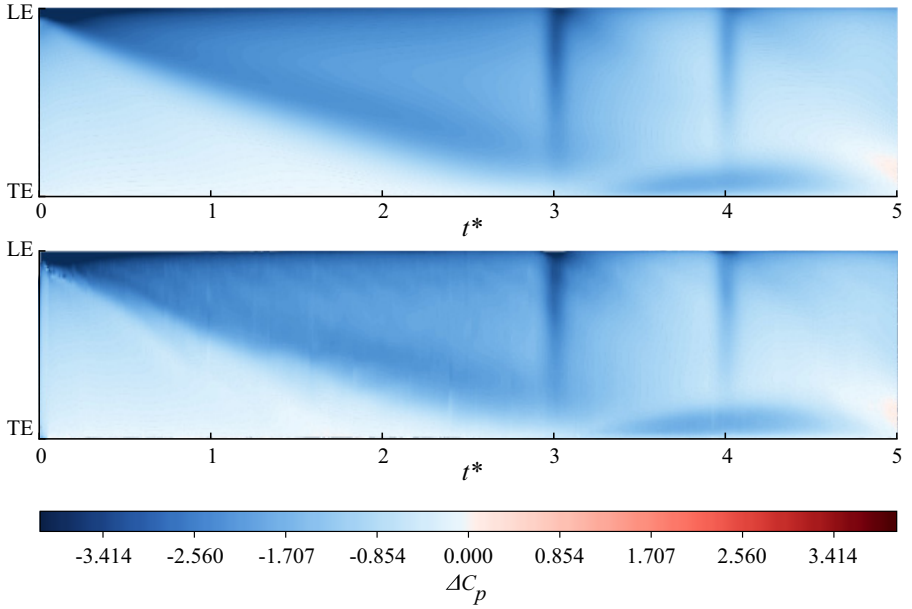

FIG. 14. Histories of the surface pressure distribution along an impulsively translating plate at 20°, subjected to incident gusts at $t^* = 3$ and $t^* = 4$, from high-fidelity truth simulation at Reynolds number 500 (top) and the EnKF-assisted model with covariance inflation (bottom).

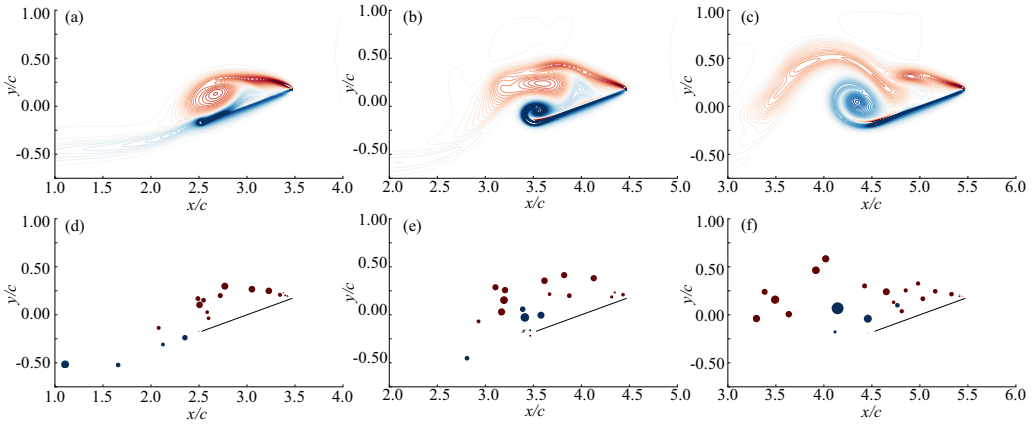

FIG. 15. Vorticity distribution for an impulsively translating plate at 20° subjected to incident gusts, at $t^* = 3$ (left column), $t^* = 4$ (center column), and $t^* = 5$ (right column), predicted by [(a)–(c)] high-fidelity truth simulation at Reynolds number 500, and [(d)–(f)] the EnKF-assisted model with covariance inflation.

This agreement in surface pressure and vorticity distribution is also manifested in the normal force exerted on the plate, shown in Fig. 16. Each gust encounter is clearly evident in the peaks observed at three and four convective times. The vortex model accurately estimates each of the peaks. It should be noted that the large spike in force soon after the motion is initiated is likely due to a spurious encounter of a vortex element with the plate. It may be possible to prevent such undesirable features by eliminating outliers in the ensemble statistics. The associated mean estimate of critical LESP is depicted in Fig. 17. This plot shows that the EnKF responds to the measured disturbances in pressure by temporarily increasing LESP_c. Since the increase in critical LESP tends to reduce vorticity flux, this small pulse in LESP_c has the effect of severing the leading-edge shear layer before developing a new LEV.

As with the previous cases, it is interesting to inspect the variances in the ensemble states. These are shown in Fig. 18, where they are compared with a noninflated version of the model. As expected, the ensemble variances of the inflated version of the model remain relatively constant. This enables the ensemble to remain responsive to measurements. However, as in the previous undisturbed case, the ensemble variances of the noninflated case quickly drop to very small values, blinding the EnKF to new observations. By three convective times, the ensemble variance in LESP_c

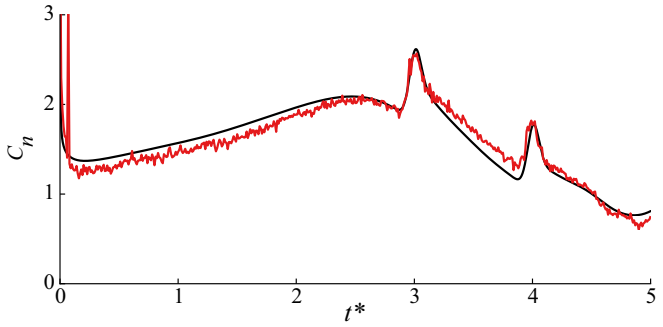

FIG. 16. Comparison of the histories of the normal force coefficient for an impulsively translating plate at 20° subjected to two incident gusts at $t^* = 3$ and $t^* = 4$, from high-fidelity truth simulation (—) and an EnKF-assisted vortex model (—).

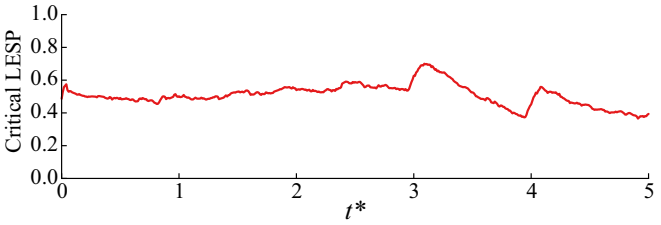

FIG. 17. Time history of the ensemble mean value of LESP_c for 20° impulsively translating plate, subjected to incident gusts at $t^* = 3$ and $t^* = 4$.

has dropped to essentially zero. When the EnKF detects the pressure signature of the disturbance, the only state parameters it can adjust are the vortex states, so we see sharp increases in the variances in the vortex states around three convective times. However, the vortex generated at the leading edge is stronger than that of the truth case, and the resulting vortex element dynamics do not accurately track the flow. Covariance inflation is essential for maintaining consistently open channels that transfer measurement discrepancies to updates in the vortex states and critical LESP.

IV. CONCLUSIONS

In this work, we have developed a dynamic estimation framework for two-dimensional unsteady separated flows, in which surface pressure measurements from the true system are used to augment a discrete vortex element model in order to predict the full state of the flow. The vortex model utilizes advecting regularized vortex elements released from the leading and trailing edges of a flat plate. At the leading edge, the strength of shed vorticity is determined by the critical leading-edge suction parameter (LESP). The estimation framework uses an ensemble Kalman filter (EnKF),

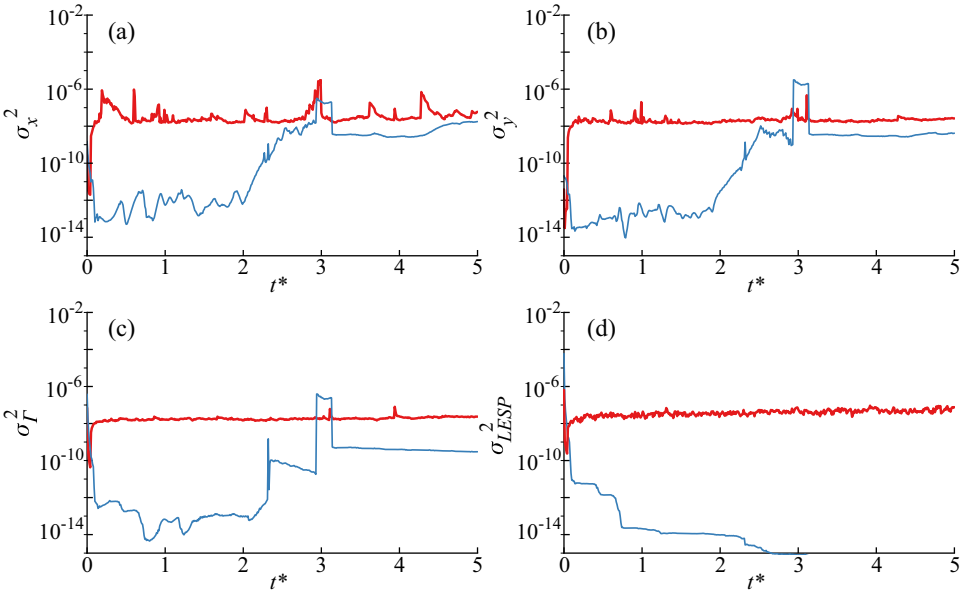

FIG. 18. Ensemble variances for the 20° impulsively translating plate, subjected to incident gusts at $t^* = 3$ and $t^* = 4$, with no covariance inflation (—) and with covariance inflation (—). Variances for (a) element x position, (b) element y position, (c) element strength, and (d) critical LESP.

in which a collection of randomly initialized vortex models are used to predict the state of the flow, continuously updated with the sampled surface pressures from the truth case. We showed that, with the appropriate tuning of the covariance inflation parameters, the ensemble of vortex element models was able to predict a vorticity and pressure distribution that closely resembles that from high-fidelity numerical simulation at Reynolds number 500. Furthermore, once we tuned the model for a single case—that of the pulse-free 20° impulsive translation case—we saw that the same covariance inflation parameters worked well for other cases, at different angle of attack or with incident disturbances.

The state vector in our implementation of the EnKF consists of the vortex positions and strengths as well as the critical LESP. It should be noted that an ensemble of size N of vortex models consisting of n_v elements each is significantly faster than a single model of Nn_v elements: Only the n_v elements in each model interact with each other, so the overall ensemble scales linearly with N rather than quadratically. Thus, even a large ensemble of models of around 30 elements each can run for five convective time units in around a minute on a laptop computer. It is also important to stress that we have no dynamical model for the critical LESP; rather, we rely only on the measured surface pressures along the plate to estimate this parameter via the Kalman gain. In so doing, we have implicitly shown that the critical LESP—that is, the tolerance of the flow to sustain relative motion of the fluid about the edge without separating—changes dynamically in response to changing flow conditions, and particularly, in response to a disturbance. This, in turn, triggers the appropriate release (and, at times, suppression) of new vorticity at the leading edge in the presence of such an aerodynamic disturbance. This demonstrates the potential for using real-time data as part of the closure model for a leading-edge shedding criterion, even in the presence of disturbances of unknown characteristics. We are currently investigating whether other forms of disturbance, such as surface actuator pulses or rigid-body excursions, can be similarly represented and observed in the critical LESP. We are also exploring the relationship between the additive covariance inflation of vortex parameters in the ensemble and the well-known random walk approach for modeling viscous diffusion in vortex methods.

In our demonstration of the estimation framework in this paper, we have relied on truth measurements from a high-fidelity numerical simulation of the flow past a flat plate. In ongoing work, we are exploring the number and location of pressure sensors that can ensure a good estimate. Furthermore, it should be stressed that the framework is agnostic to the source of the truth measurements. This aspect is especially important as the framework serves its intended use in real-time flow control. Ultimately, we seek to replace these numerically computed pressure measurements with sampled experimental measurements.

ACKNOWLEDGMENTS

Support by the US Air Force Office of Scientific Research (Grant No. FA9550-14-1-0328) is gratefully acknowledged. A.F.d.C. would like to thank the Ministry of Education of Brazil (Capes Foundation) for its support through a Science without Borders scholarship (Grant No. BEX 12966/13-4).

APPENDIX: VORTEX AGGREGATION PROCEDURE

The vortex aggregation procedure used in this work is a modified version of the hybrid vortex sheet-point vortex model developed by Darakananda and Eldredge [9]. In the hybrid model, the leading- and trailing-edge shear layers are each modeled as a vortex sheet rooted near the respective edge. At every time step, circulation from the free end of a vortex sheet is siphoned into a variable-strength point vortex. To prevent this instantaneous transport of circulation from adversely affecting the aerodynamic force response, the velocity of the variable-strength point vortex is adjusted based on an impulse matching principle developed by Wang and Eldredge [8]. The adjustment comes in the form of a velocity correction, added to the usual Kirchhoff velocity of a vortex element obtained

through Biot-Savart summations. For later description, let us label each of these consumed elements on the sheet as the "source" (with subscript s) and the variable-strength element as the "target" (with subscript t). The velocity correction of the target element, $\Delta\dot{z}_t = \Delta\dot{x}_t + \mathrm{i}\Delta\dot{y}_t$, written in complex notation for brevity, is

$$\Delta\dot{z}_t = ie^{i\alpha}\frac{c}{2}\left[\frac{(\tilde{p}_s - \tilde{p}_t)(\beta^\star + 1) + (\tilde{p}_s^\star - \tilde{p}_t^\star)(\beta^\star - 1)}{\beta + \beta^\star}\right]\frac{\dot{\Gamma}}{\Gamma_t}, \tag{A1}$$

where $\dot{\Gamma}$ is the rate of transfer of circulation from the source to the target, Γ_t is the instantaneous target element strength, $()^\star$ denotes complex conjugation, and, for i either s (source) or t (target), the unit impulse (accounting for the influence of the plate) is

$$\tilde{p}_i := \mathrm{Im}\{\tilde{z}_i\} - i\mathrm{Re}\{\sqrt{\tilde{z}_i - 1}\sqrt{\tilde{z}_i + 1}\}$$

and the gradient of the target's impulse with respect to its position is

$$\beta := \frac{\tilde{z}_t}{\sqrt{\tilde{z}_t - 1}\sqrt{\tilde{z}_t + 1}}.$$

In each time step, the strengths of successive source elements are transferred into the target until a threshold on error (the spurious change to the predicted aerodynamic force on the plate due to the transfer) is reached. When it becomes impossible to transfer any circulation from the sheet without exceeding the threshold, the target element turns into a classical constant-strength vortex and the tip of the vortex sheet is converted into a new variable-strength point vortex, i.e., a new target. The connectivity maintained between elements in the sheet makes it always clear which vortex element consumes circulation and which one supplies it.

By using unconnected discrete vortex elements instead of connected vortex sheets, we lose the natural ordering of the vortex elements that was provided by the sheets, and thus, we lack an unambiguous relationship between vortex elements that can be exploited for aggregating these elements. Instead, we will take the most straightforward approach and simply test every possible combination of source-target pairs to determine which pairwise transfer will incur the least error in predicted force. We then perform the transfer on as many pairs as possible while keeping the accumulated error below a specified threshold, ϵ_F. Once we have set an appropriate value for ϵ_F, we do the following at every time step:

(1) For every possible source-target pair of vortex elements in the model, use Eq. (A1) to compute and store the hypothetical velocity correction to the target required if all of the source's circulation is transferred into the target.

(2) Compute the (uncorrected) velocities of all vortex elements and evolve the system forward by one time step.

(3) Compute the impulse for each vortex element at this end of this step.

(4) For every possible source-target pair of vortex elements in the system, first determine, from the velocity correction computed in step 1, the hypothetical impulse that the target element would have if it had absorbed all the circulation from the source element. Subtract from this the actual impulse of the source and target elements, computed in step 3. This difference, when divided by time-step size, is defined as the transfer error and is a measure of the spurious force on the plate due to the aggregation.

(5) Sort the source-target pairs based on the magnitude of their transfer error.

(6) Starting from the pair with the lowest error, transfer circulation between as many pairs of vortex elements as possible, stopping just before the accumulated error exceeds ϵ_F.

This aggregation procedure naturally favors merges between elements of similar significance to force generation. Many such element pairs are closely separated, but not all closely separated pairs are merged: For example, two nearby elements of opposite-signed strength or widely different velocities may not be merged by these criteria.

Although the procedure listed above contains multiple steps, with pairwise interactions that are usually undesirable, it also serves to prune a significant number of vortex elements in the system. In practice, the computational savings of keeping the state's dimensionality small far outweighs the cost of executing this procedure at every time step. The cost of a similar procedure was analyzed in detail in Ref. [9].

[1] X. An, D. R. Williams, J. D. Eldredge, and T. Colonius, Modeling dynamic lift response to actuation, 54th AIAA Aerospace Sciences Meeting, San Diego, CA, AIAA Paper 2016-0058, 2016 (unpublished).

[2] S. A. Ansari, R. Zbikowski, and K. Knowles, Non-linear unsteady aerodynamic model for insect-like flapping wings in the hover. Part 2: Implementation and validation, Proc. Inst. Mech. Eng. Part G J. Aerosp. Eng. **220**, 169 (2006).

[3] K. Ramesh, A. Gopalarathnam, K. Granlund, M. V. OL, and J. R. Edwards, Discrete-vortex method with novel shedding criterion for unsteady aerofoil flows with intermittent leading-edge vortex shedding, J. Fluid Mech. **751**, 500 (2014).

[4] X. Xia and K. Mohseni, Lift evaluation of a two-dimensional pitching flat plate, Phys. Fluids **25**, 091901 (2013).

[5] C. E. Brown and W. H. Michael, Effect of leading-edge separation on the lift of a delta wing, J. Aeronaut. Sci. **21**, 690 (1954).

[6] S. Michelin and S. G. Llewellyn Smith, An unsteady point vortex method for coupled fluid–solid problems, Theor. Comput. Fluid Dyn. **23**, 127 (2009).

[7] A. Tchieu and A. Leonard, A discrete-vortex model for the arbitrary motion of a thin airfoil with fluidic control, J. Fluids Struct. **27**, 680 (2011).

[8] C. Wang and J. D. Eldredge, Low-order phenomenological modeling of leading-edge vortex formation, Theor. Comput. Fluid Dyn. **27**, 577 (2013).

[9] D. Darakananda and J. D. Eldredge, A versatile taxonomy of low-dimensional vortex models for unsteady aerodynamics, J. Fluid Mech. **858**, 917 (2019).

[10] D. Darakananda, J. D. Eldredge, T. Colonius, and D. R. Williams, A vortex sheet/point vortex dynamical model for unsteady separated flows, 54th AIAA Aerospace Sciences Meeting, San Diego, CA, AIAA Paper 2016-2072, 2016 (unpublished).

[11] J. Katz, A discrete vortex method for the non-steady separated flow over an airfoil, J. Fluid Mech. **102**, 315 (1981).

[12] K. Ramesh and A. Gopalarathnam, Theoretical modeling of leading edge vortices using the leading edge suction parameter, 30th AIAA Applied Aerodynamics Conference, New Orleans, LA, AIAA Paper 2012-3027, 2012 (unpublished).

[13] 13 M. S. Hemati, J. D. Eldredge, and J. L. Speyer, Improving vortex models via optimal control theory, J. Fluids Struct. **49**, 91 (2014).

[14] J. D. Eldredge and D. Darakananda, Reduced-order two- and three-dimensional vortex modeling of unsteady separated flows, 53rd AIAA Aerospace Sciences Meeting, Kissimmee, FL, AIAA Paper 2015-1749, 2015 (unpublished).

[15] G. Evensen, Sequential data assimilation with a nonlinear quasi-geostrophic model using Monte Carlo methods to forecast error statistics, J. Geophys. Res. **99**, 10143 (1994).

[16] A. F. C. da Silva and T. Colonius, Ensemble-based state estimator for aerodynamic flows, AIAA J. **56**, 2568 (2018).

[17] A. Gelb, *Applied Optimal Estimation* (MIT Press, Cambridge, MA, 1974).

[18] G. Burgers, P. Jan van Leeuwen, and G. Evensen, Analysis scheme in the ensemble Kalman filter, Mon. Weather Rev. **126**, 1719 (1998).

[19] J. L. Anderson and S. L. Anderson, A Monte Carlo implementation of the nonlinear filtering problem to produce ensemble assimilations and forecasts, Mon. Weather Rev. **127**, 2741 (1999).

[20] P. J. van Leeuwen, Comment on "Data assimilation using an ensemble Kalman filter technique," Mon. Weather Rev. **127**, 1374 (2010).
[21] J. S. Whitaker and T. M. Hamill, Evaluating methods to account for system errors in ensemble data assimilation, Mon. Weather Rev. **140**, 3078 (2012).
[22] G. Evensen, *Data Assimilation: The Ensemble Kalman Filter* (Springer Science & Business Media, Berlin, 2009).
[23] K. Taira and T. Colonius, The immersed boundary method: A projection approach, J. Comput. Phys. **225**, 2118 (2007).
[24] M. A. Jones, The separated flow of an inviscid fluid around a moving flat plate, J. Fluid Mech. **496**, 405 (2003).
[25] A. J. Chorin, Numerical study of slightly viscous flow, J. Fluid Mech. **57**, 785 (1973).